Sensors and Materials, Vol. 36, No. 8 (2024) 3539–3555
MYU Tokyo

S & M 3749

Intelligent Laser Photolysis System

Yuan-Hong Guan,[1] Meng-Sheng Tsai,[1] Chung-Yi Pan,[2]
Jan Pan Hwang,[3] and Meng-Hua Yen[1*]

[1]Department of Electronic Engineering, National Chin-Yi University of Technology, Taichung 41170, Taiwan
[2]Asia Power Laser Maker Co., Ltd., Taichung 40761, Taiwan
[3]Department of Information Management, National Chin-Yi University of Technology, Taichung 41170, Taiwan

(Received October 30, 2023; accepted July 4, 2024)

Keywords: CO_2 laser, 2D LiDAR, photothermal laser ablation, high-power laser

Traditional waste incineration generates a large amount of exhaust gas, resulting in adverse environmental impacts. Therefore, we developed an organic and intelligent photochemical processing system that utilizes high-energy lasers for incineration, thereby reducing the production of exhaust gas. A large-scale laser machine was set up, incorporating low-cost 2D Light Detection and Ranging (LiDAR) technology for system sensing, which performs angle range and threshold filtering, as well as multispectral laser allocation, integrated with the laser ablation machine system. After testing, the error was <5 mm (<8%), achieving precise object scanning and ranging and solving the problem of manual laser positioning. Experimental results showed that CO_2 lasers can effectively process organic materials and medical waste of different sizes. This innovative research will have profound implications for the future development of environmental protection and incineration technologies. In the future, it has widespread application prospects in areas such as pet waste disposal and medical waste treatment.

1. Introduction

With the rise of environmental awareness today, in this study, we aim to fully utilize the advantages of laser technology for the ablation of both organic and inorganic materials. *Laser light* is a highly focused, high-energy beam produced by a particular light source. The characteristics of laser light include a single wavelength, high coherence, strong directionality, and a narrow beam. These features have led to its widespread application in various fields, including medical aesthetics, manufacturing, and engraving.[1–3] Several reasons underpin our choice of using laser light for object vaporization technology. Traditional incineration produces a significant amount of exhaust gases during combustion. The emission of these gases can adversely impact the environment, leading to a rapid increase in carbon dioxide and organic dust concentrations.[4–6]

Moreover, the emitted gases can severely harm humans.[7] However, the instantaneous high-energy evaporation treatment using laser light can rapidly fragment or even melt objects,[8,9] thereby reducing the processing time and minimizing the harm of exhaust gases to the

*Corresponding author: e-mail: emh1989@ncut.edu.tw
https://doi.org/10.18494/SAM4744

ISSN 0914-4935

environment and humans during combustion. The potential of laser light in waste management, including organic materials and medical waste, is significant and might even replace traditional crematoriums. Especially when dealing with mass casualties caused by large-scale disasters or epidemics, more than conventional incineration might be needed to meet the rapid processing demands.

As an example, the COVID-19 pandemic has had a profound impact globally, with hundreds of millions infected and hundreds stagnated owing to its effects. This has placed immense pressure on crematoriums, which cannot handle the high daily death toll. In some regions, crematoriums are overwhelmed to the point of not operating sufficiently, with morgues and funeral homes overburdened. For instance, when handling COVID-19 casualties, crematoriums in India have limited speed, sometimes taking up to 90 min to cremate a single body. The increasing need for critical equipment or a new incineration method becomes crucial in such circumstances.

Moreover, the cremation process releases many microbial air pollutants, including particulates, nitrogen dioxide, nitrogen oxides, volatile organic compounds, and heavy metals. These pollutants may severely impact the environment and human health.[10] Additionally, African Swine Fever (ASF) spread rapidly in Asia and was confirmed in Mongolia on January 10, 2019.[11] Incineration or refining is the most effective and straightforward method when handling infected carcasses. Dead animals are buried in holes at least two meters deep outside residential areas and incinerated with highly flammable materials such as gasoline and tires. Given the climatic conditions during the outbreak, carcasses are either entirely or sometimes only partially burned to ashes.[12] If not fully incinerated before burial, there might be environmental pollution concerns. Therefore, innovative approaches are needed in traditional waste management processes to ensure more thorough incineration on a large scale, effectively reducing ecological damage, and strict system monitoring should be implemented by law.

Amid the COVID-19 pandemic, the increased use and improper disposal of personal protective equipment (PPE) have resulted in significant medical waste. The most effective way to handle this waste is through incineration, which requires at least 60 min and emits exhaust gases.[13,14] The inability to process this waste rapidly underscores the importance of managing medical waste. However, one-third of healthcare facilities worldwide lack waste segregation systems, and in the least developed countries, fewer than one-third of healthcare institutions have essential medical waste management services.[15] According to annual statistics, 4 million children die from diseases related to poor medical waste management.[16]

Additionally, when medical waste is incinerated, it produces substances such as dioxins, furans, and particulates.[17] Reports indicate that in some regions of Nepal, PPE was left around vaccination sites and openly burned, posing health and environmental risks. The World Health Organization states that air pollution and carcinogens from waste incineration are among the most significant risks societies face.[15] By accelerating the processing of medical waste, reducing incineration and storage time, and implementing effective recycling management, the spread of infectious diseases due to medical waste can be effectively reduced.

We developed an intelligent photolysis machine for organic entities, and we conducted laser incineration experiments on general objects and waste materials. By utilizing this platform and

the high energy density of lasers, the rapid photolytic treatment of objects can be achieved, effectively addressing the air pollution issues associated with traditional incineration methods. It provides a faster, more environmentally friendly, and more precise approach to object incineration. This technology holds potential in waste management and resource recycling, significantly promoting sustainable environmental development.

2. Materials and Methods

2.1 Laser vaporization equipment

We developed a large laser platform with dimensions of 346 cm in length, 230 cm in width, and 240 cm in height, designed explicitly for the photovaporization of solid objects. This platform boasts impressive processing capabilities, able to vaporize objects up to 120 cm in length, 50 cm in width, and 60 cm in height. The platform integrates several core components, including a CO_2 laser, a laser spectroscopy system, a HEPA air filtration exhaust system, a platform elevation system, a motor controller, and a 2D Light Detection and Ranging (LiDAR) device, to achieve efficient photovaporization. These components play crucial roles during photovaporization, as illustrated in Figs. 1 and 2.

The platform is equipped with a 4000 W CO_2 laser from Rofin, which is capable of delivering high-power output for the laser light vaporization of objects. This CO_2 laser boasts exceptional stability and reliability, allowing for the precise adjustment and control of the laser beam to cater

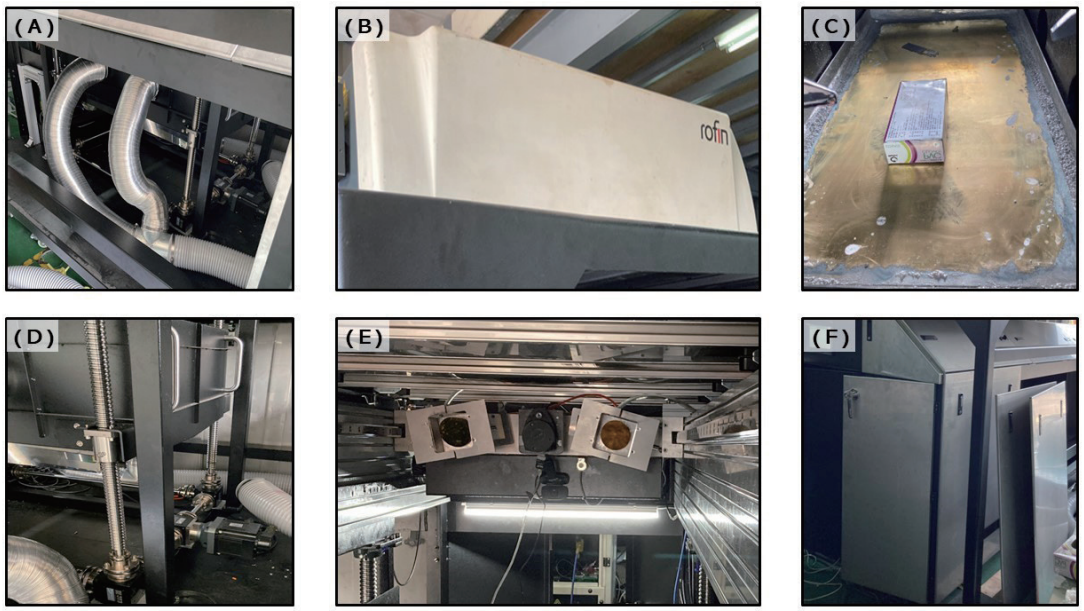

Fig. 1. (Color online) Core components of the laser light vaporization platform. (A) HEPA air filtration exhaust system, (B) Rofin CO_2 laser, (C) brass material platform, (D) platform elevation system, (E) laser spectroscopy system, and (F) S45C medium carbon steel material.

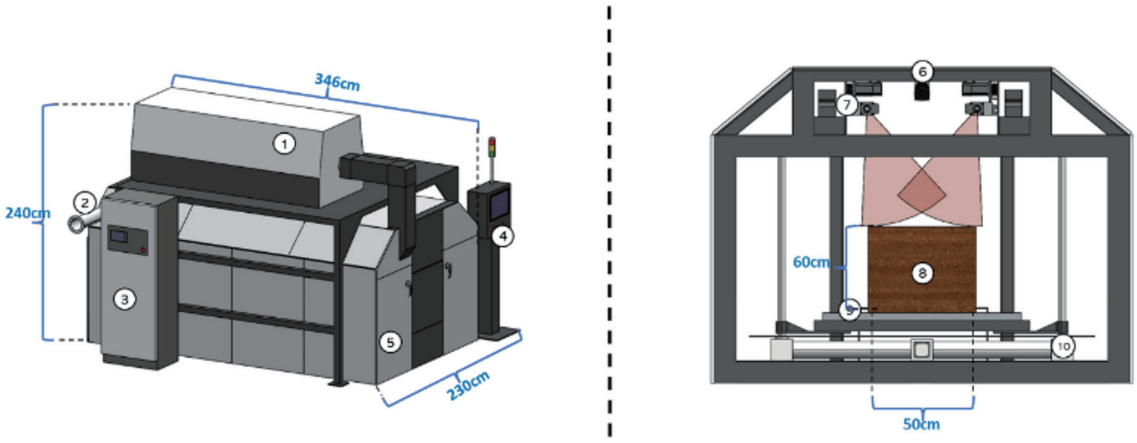

Fig. 2. (Color online) System simulation diagram. On the left are (1) a Rofin CO_2 laser, (2) a HEPA air filtration exhaust system, (3) a system control box, (4) a control panel, (5) an S45C medium carbon steel material, (6) a 2D LiDAR device, (7) a laser spectroscopy system, (8) an object awaiting vaporization system, (9) a brass material platform, and (10) a platform elevation system.

to the photovaporization of various materials. The laser spectroscopy system used by the machine further enhances the incineration efficiency of the laser vaporization platform. Utilizing the concept of spectroscopy, the laser beam is directed onto two sets of parabolic mirrors inside the furnace. These two mirrors, controlled by motors, can rotate within a range of plus or minus 45 deg.

The laser spectroscopy system is also mounted on a linear rail inside the furnace. Such a design enables the platform to process large-area objects rapidly, significantly improving the efficiency of photovaporization. During the laser light vaporization, the generated suspended particles and harmful gases pose potential risks to the working environment and the safety of operators. The platform is equipped with a HEPA air filtration exhaust system to ensure a clean working environment and the safety of operators. This system effectively filters and removes suspended particles and harmful gases, ensuring good indoor air quality.

Moreover, the platform is also equipped with an elevation system, which collaborates with a 2D LiDAR device. The 2D LiDAR device can model objects and convert the measured data to achieve accurate object positioning[18] while also realizing the laser's autofocus function. This positioning ensures that the laser beam is precisely focused on the target object, guaranteeing the accuracy of photovaporization.

In the initial stages of the experiment, the photolysis reactions of organic materials were tested using fiber and CO_2 lasers. The fiber laser has a wavelength of 1064 nm. Organic materials have a lower absorption rate for this type of laser, leading to carbonization during photovaporization and consequently increasing the time required for photovaporization. The CO_2 laser has a wavelength of 10600 nm, which is effectively absorbed by organic materials,[19,20] making it a more suitable choice for the photovaporization of organic materials. Additionally, to prevent potential hazards during photovaporization, such as high temperatures, laser exposure, and dust, S45C medium carbon steel was used to seal the internal processing area, thereby preventing accidents. Owing to the extremely high power density at the laser's focal point, the

heat input from the beam far exceeds the portion reflected, conducted, or diffused by the material, causing the material to rapidly heat to a vaporization level, resulting in evaporative pitting. The bottom platform should be made of a material that can withstand high-power lasers for extended periods to prevent damage to the platform by the laser. Considering using the CO_2 laser as the source, we chose brass as the base material. The 2D LiDAR device, used for object scanning calculations and positioned directly above the reflection point of the base material, was also protected with a metal workpiece.

In summary, the laser light vaporization platform system used in this study not only integrates our previous research achievements ("Realization of laser object vaporization locating based on low-cost 2D LiDAR"),[21] but also successfully combines critical components such as high-power CO_2 lasers, laser spectroscopy systems, HEPA air filtration exhaust systems, platform elevation systems, motor controllers, and 2D LiDAR devices. Furthermore, using medium carbon steel and brass as the primary materials for the system aids in ensuring the platform's durability and safety, providing appropriate material properties to handle the high temperatures and laser energy generated during photovaporization, as shown in Fig. 3. The configuration and provision of these designs and components enable the platform to efficiently process large-area objects while ensuring a clean working environment and the safety of operators. This allows our study to achieve outstanding results in photovaporization applications.

2.1.1 System operation procedure

The operator examines the system status to ensure that the laser platform is in standby mode, indicating that the machine is ready and can accept commands. Next, the object to be processed is placed inside the furnace. Laser parameters are adjusted within the graphical user interface (GUI), including object size, speed, and power, to achieve optimal photovaporization results.

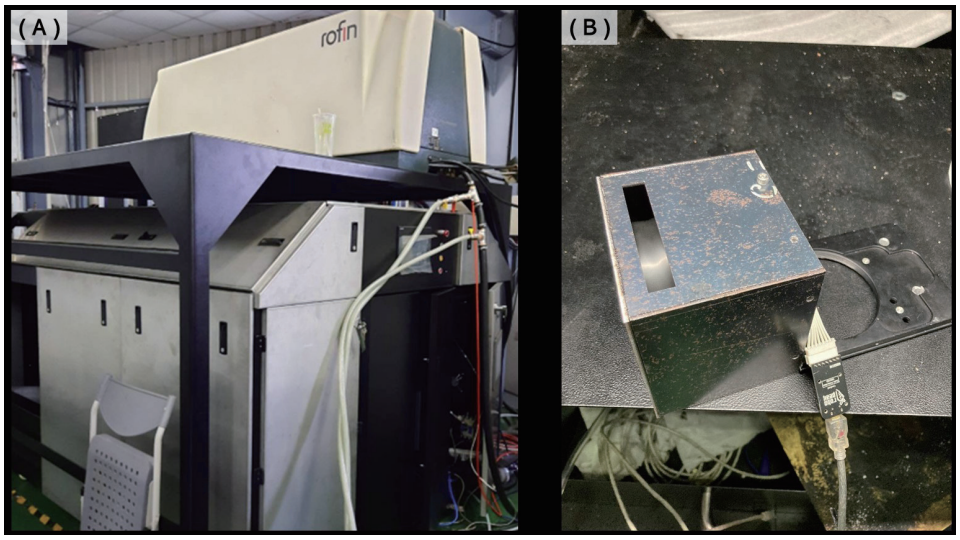

Fig. 3. (Color online) Physical image of the multispectroscopy laser vaporization system. Physical images of the (A) platform and (B) 2D LiDAR device, which is protected by a metal workpiece.

Once the parameters are set, pressing the button can initiate laser photovaporization. Simultaneously with this photovaporization, the 2D LiDAR device begins scanning the object and generates the corresponding 2D modeling diagram. The laser platform adjusts the laser focus and the angle of the multispectroscopy laser on the basis of the 2D modeling information, performing the laser vaporization operation on the object. After the photovaporization, the GUI status area displays that the laser platform has finished the process. The operator then pushes the residues of the vaporized object into a storage box while cleaning the inside of the furnace, preparing for the next photovaporization operation. Finally, the storage box is removed, completing the photovaporization, as shown in Fig. 4. This procedure ensures the system's smooth operation, guaranteeing the efficiency and safety of the photovaporization operation.

2.1.2 System communication integration and information transmission

In the system integration part, we integrated the laser platform, air filtration device, various sensors, and 2D LiDAR device into the system's GUI interface. Moreover, on the basis of our previous research results,[21] communication between the PC side and the laser hardware side [programmable logic controller (PLC)] was established using Modbus TCP.

After confirming that the system is successfully connected, the operator places the item to be vaporized in the vaporization furnace, ensuring safety and accuracy. Then, the system activates the 2D-LiDAR device, starting a precise scanning operation on the object. The PC and laser exchange information in real time during scanning, as seen in Fig. 5. At the same time, the Y-axis of the laser device is activated, driving the 2D-LiDAR device to move precisely on the object's surface. By obtaining the height information of the object from various angles, the system can accurately calculate the width of the target object. This positioning data is transmitted from the PC to the PLC to record the operational data of the target object during the vaporization.

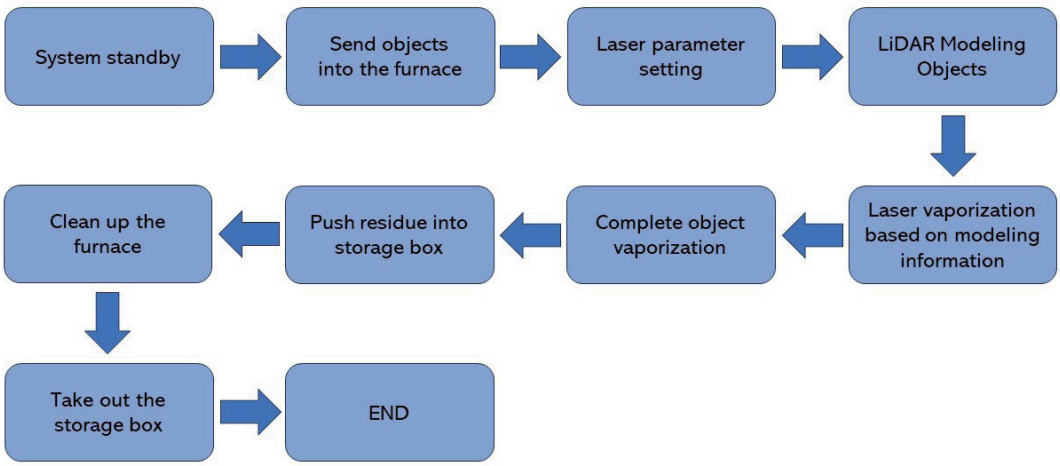

Fig. 4. (Color online) System operation flowchart.

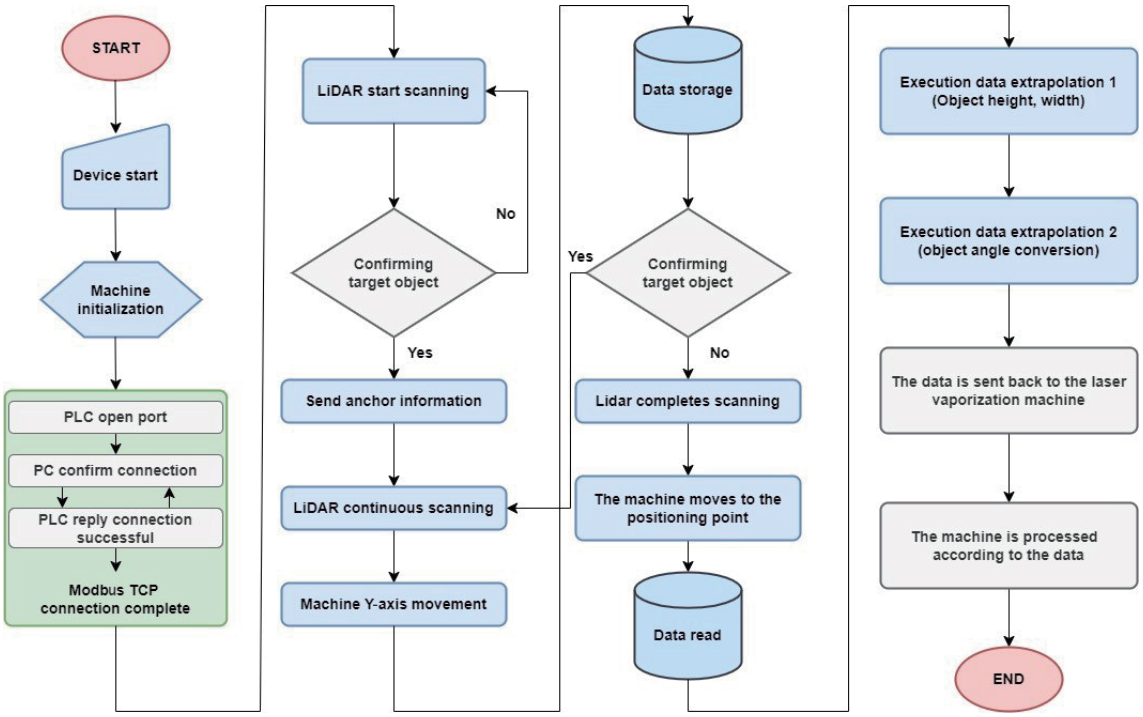

Fig. 5. (Color online) Communication and scanning workflow between 2D LiDAR device and laser platform.

After scanning, the system will execute the vaporization operation on the basis of pre-entered laser parameters. The rotation angle of the multispectroscopic laser will be accurately calculated using the cosine theorem to achieve precise vaporization effects. This ensures that the two light beams can ideally target the object after spectroscopy, achieving accurate vaporization results.

The entire communication and scanning workflow between the 2D LiDAR device and the laser platform is detailed in Fig. 5, showcasing the close collaboration and exact operation between processes. This system's workflow design aims to ensure the reliability and efficiency of the vaporization, providing reliable technical support for targeted vaporization treatment.

2.1.3 User interface

The GUI designed for this study is shown in Fig. 6. It was developed and designed using C# software, offering an intuitive and user-friendly environment. This interface is divided into four main sections: the machine status area, the laser parameter settings area, the 2D LiDAR modeling diagram, and the operation area.

The top left section of the interface is the machine status area. This area displays the operational status of the laser machine, including three states: machine standby, machine vaporization, and machine vaporization complete. The machine standby status indicates that the laser machine is currently idle and not performing any actions, signifying that the machine is ready and can accept any commands. The machine vaporization status indicates that the laser

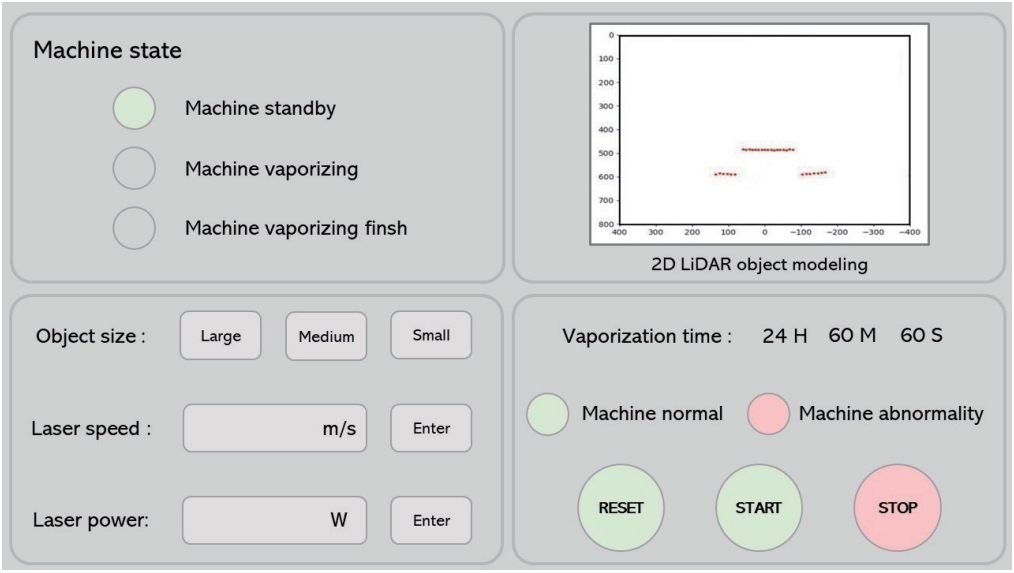

Fig. 6. (Color online) User interface.

machine is in the process of vaporization and actively vaporizing the target object. The machine vaporization complete status means that the laser machine has finished the vaporization, signifying that the vaporized object can be removed or the machine is ready for the next vaporization task.

The bottom left section of the interface is the laser parameter settings area. Operators can set parameters such as object size, laser speed, and power within this area. These parameters can be adjusted on the basis of vaporization requirements and material characteristics to achieve the best results.

The top right section of the interface displays the 2D LiDAR modeling diagram, which shows the object modeling diagram captured by the 2D LiDAR device. This modeling diagram is presented in a 2D format, displaying information such as the object's shape, contour, and position, allowing operators to better understand the object's geometric features and positional relationships.

The bottom right section of the interface is the operation area, which includes a start button, an emergency stop button, and a reset button. Pressing the button initiates the vaporization; once pressed, the machine will begin vaporization based on the set parameters. The emergency stop button is designed to immediately stop the machine's operation, addressing any unexpected or urgent situations. The reset button is used to reset the status and parameters of the laser machine. Additionally, the operation area displays the vaporization time and the machine's status. The vaporization time indicates the duration of the ongoing vaporization, providing operators with control over the process. The machine status displays the current operating state of the laser machine, including regular operation or any alerts for anomalies. If there is an anomaly with the machine, the operation area will display the corresponding error message, alerting the operator to the issue.

2.2 Applications of 2D LiDAR devices

This section of the research is primarily based on our previous findings.[21] We used a 2D LiDAR device to model objects and calculate their height and subsequently used this height information to autofocus the laser machinery. For this device, we chose the RPLIDAR A1M8 developed by SLAMTEC; the detailed technical specifications are provided in Table 1. RPLIDAR A1M8 is a low-cost 360° 2D LiDAR device suitable for cost-effective object positioning and development, as shown in Fig. 7. To integrate it into the laser vaporization system, we rotated it at an angle of 90° and mounted it on the laser vaporization machine. Measurements were taken using a universal angle gauge for the long sides of both the setup platform and the LiDAR device, where the mechanical precision of the universal angle gauge is ±0.2°. This ensured that the relative angle between the LiDAR device and the platform was 90°, and the angle gauge was then utilized to measure the relative angle between the LiDAR device and the two laser heads on either side to ensure parallelism. Furthermore, we set its scanning range to +23 to −23°, allowing for a comprehensive scan of objects on the platform.

2.2.1 2D LiDAR angle range and threshold value selection

In this study, we converted the polar coordinates (r, θ) measured by the LiDAR device into Cartesian coordinates (x, y) to model the object. Here, θ represents the angle between the object and the LiDAR device, and r represents the distance corresponding to that angle. This conversion allows us to obtain all the (x, y) points of the object on the platform, as shown in Eq. (1). This algorithm is consistent with our previous research results.[21]

Given that the platform of this system has a specific curvature and is not entirely flat, in order to enhance detection stability in this study, we set a critical boundary value during the scanning movement called the platform threshold, which is set at 30 mm. Subsequently, the Cartesian distance is calculated. The Cartesian distance represents the vertical distance between the object and the LiDAR device, which can be derived from the object's Cartesian coordinates. Each scanned angle provides a Cartesian distance. The presence of an object can be determined

Table 1
2D LiDAR detailed technical specifications.

Item	Unit	Typical	Comments
Distance range	Meter (m)	0.15–12	White objects
Angular range	Degree	0–360	
Scan field flatness	Degree		
Distance resolution	mm	<0.5	<1.5 m
		<1% of the distance	Distance range*
Angular resolution	Degree	≤1	5.5 Hz scan rate
Sample duration	Milliseconds (ms)	0.125	
Sample frequency	Hz	≥8000	
Scan rate	Hz	5.5	Typical value is measured when RPLIDAR A1 takes 360 samples per scan.

* refers to the entire range of LiDAR, that is, 0.15–12 m.

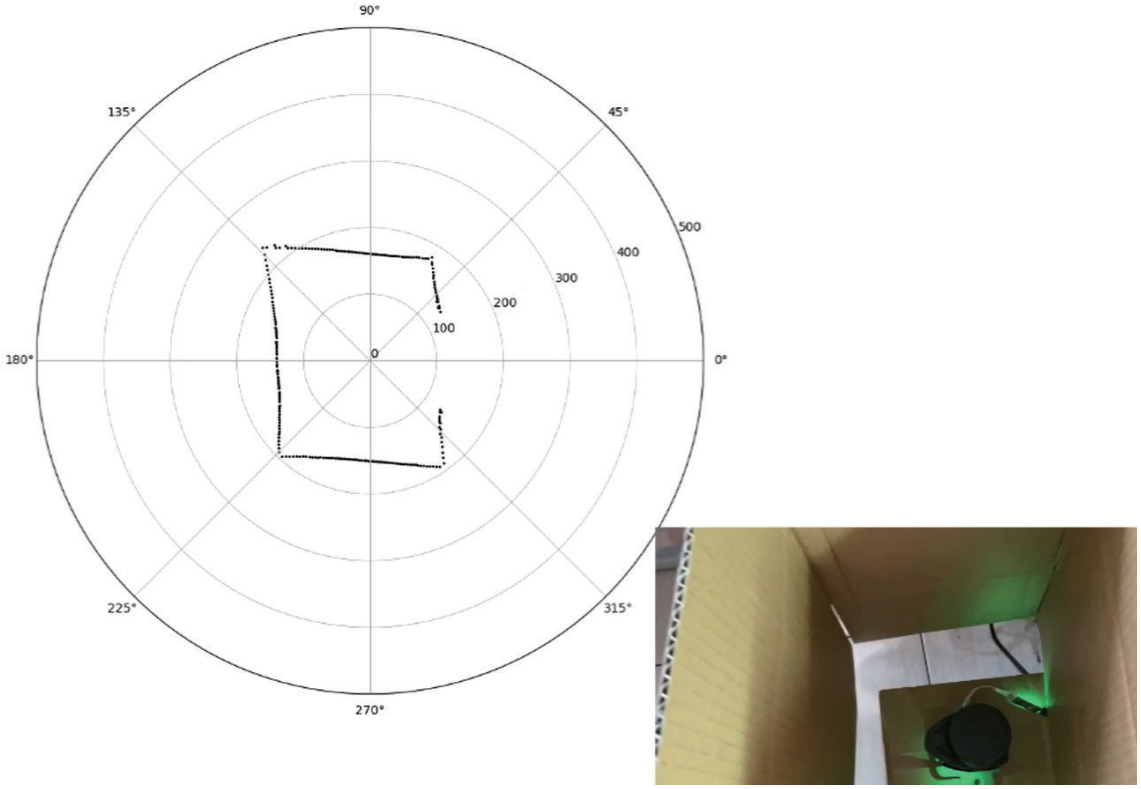

Fig. 7. (Color online) Schematic diagram of 2D-LiDAR scanning.

by calculating the difference between the Cartesian distance and the elevation platform height. If the difference is less than the platform threshold, the absence of an object is indicated. Conversely, if the difference exceeds the platform threshold, the presence of an object is signified, as shown in Eq. (2) and Fig. 8.[21] Once an object on the platform is detected, the original polar coordinates are used again to determine the object's position within the angular range of the LiDAR device, facilitating further allocation of the laser angle.

$$(x, y) = (r\cos\theta, r\sin\theta) \tag{1}$$

$$Platform\ Threshold \geq \ |Cartesian\ distance - platform| \tag{2}$$

2.2.2 Angle allocation conversion of 2D LiDAR

In this study, we adopted a multibeam laser system that can split a single laser beam into two to enhance the incineration efficiency of the system. The two laser beams are set equidistant on both sides of the LiDAR device, with the distance between them represented by the spectral laser distance. Before vaporizing the object with the laser, the rotation angle of the beam splitter should be calculated. The cosine theorem is used for this purpose, as shown in Fig. 9. First, the

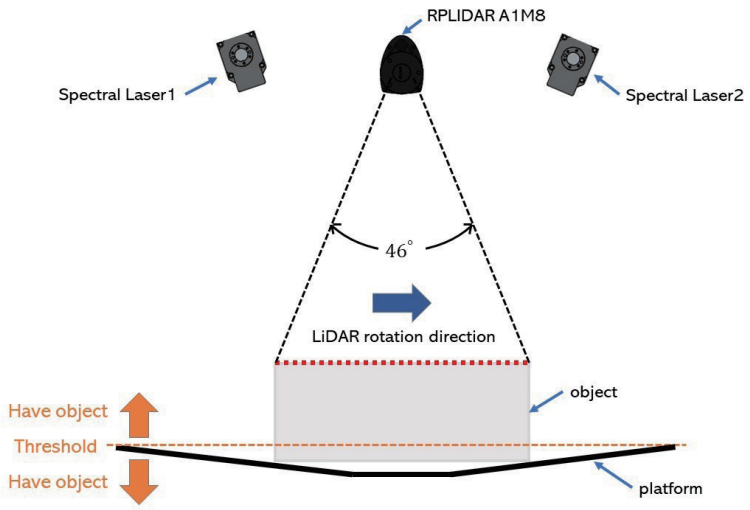

Fig. 8. (Color online) Schematic diagram of target object detection using 2D LiDAR device.

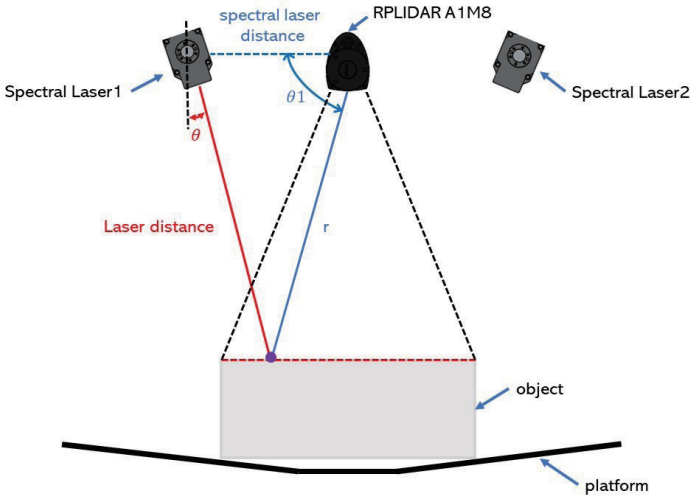

Fig. 9. (Color online) Schematic diagram of laser rotation after cosine conversion.

LiDAR device measures the polar coordinates (r, θ) of a specific point on the object. Then, using Eq. (3), the laser distance to that particular point is derived from the polar coordinates (r, θ) and the spectral laser distance. Once the laser distance is calculated, it is plugged into Eq. (4) to determine the rotation angle θ of the beam splitter, as described in previous literature.[21] Taking the actual setup method of this study as an example, where the spectral laser distance is 200 mm, the θ_1 scanning angle is 60 deg, and r is equal to 300 mm, according to Eq. (3), the laser distance is calculated to be 264.58 mm. Subsequently, by substituting these values into Eq. (4), θ is

determined to be 10.9 degrees, thus obtaining the rotation angle of the laser. This means that the rotation angle of the laser is floating. The conversion based on the relative distance relationship between the 2D LiDAR and the spectral laser can make the point actually scanned by the 2D LiDAR device become the actual position of the spectral laser.

Through precise conversion methods, we can ensure that the two beams, after beam splitting, accurately target the area where the object is located. Such design and conversion strategies enhance the system's performance and accuracy, achieving a more efficient object incineration.

This conversion method ensures that the angles and directions of the two split laser beams accurately correspond to the object's position, thereby achieving precise laser targeting. Laser targeting is especially important during the incineration, as it ensures the effective projection and distribution of incineration energy, enhancing the efficiency and uniformity of the burn.

$$laser\ distance = \sqrt{r^2 + spectral\ laser\ distanc^2 - 2 \cdot r \cdot spectral\ laser\ distance \cdot \cos\theta_1} \tag{3}$$

$$\theta = 90 - \cos^{-1} \cdot \frac{spectral\ laser\ distanc^2 + (laser\ distance)^2 - r^2}{2 \cdot spectral\ \ laser\ distance \cdot laser\ distance} \tag{4}$$

3. Results

In this study, we focused on controlling the LiDAR device and successfully integrated it into the multibeam laser vaporization platform during testing. It achieved precise target positioning and in-range tracking, verifying the accuracy of 2D LiDAR positioning. Although the curvature of the platform introduced challenges in detecting small-depth targets, the system still met the application requirements and achieved the product data standards.

For the control of RPLIDAR A1M8, the Adafruit RPLIDAR library in Python was adopted to achieve the motion control of the LiDAR device. During the testing phase, by integrating the RPLIDAR A1M8, we successfully incorporated it into the multibeam laser vaporization platform, precisely positioning the target object and tracking it within its range. Figure 10 shows the graphical state when the target object was detected. In our experiment, we tested a toolbox measuring 100 mm in width and 40 mm in height to verify the positioning results of the RPLIDAR A1M8. The results showed dimensions of 103 mm in width and 42 mm in height, with a conversion error of <5 mm; the error in width and height is less than 8%, proving the accuracy of the 2D LiDAR positioning in this research.

Moreover, during the testing phase, it was found that the range and scanning rate of the RPLIDAR A1M8 met the product data standards provided by SLAMTEC, fully satisfying the system's application requirements. Additionally, owing to the curvature in the design of the vaporization platform, objects with a smaller depth (approximately <30 mm) might need to be noticed. However, in the experimental results, the system could still locate target objects accurately and perform the corresponding laser vaporization actions for target objects with sufficient depth.

Additionally, in this study, we took organic matter as an example to explore the effects of photovaporization technology on derivative processing. CO_2 lasers were used for

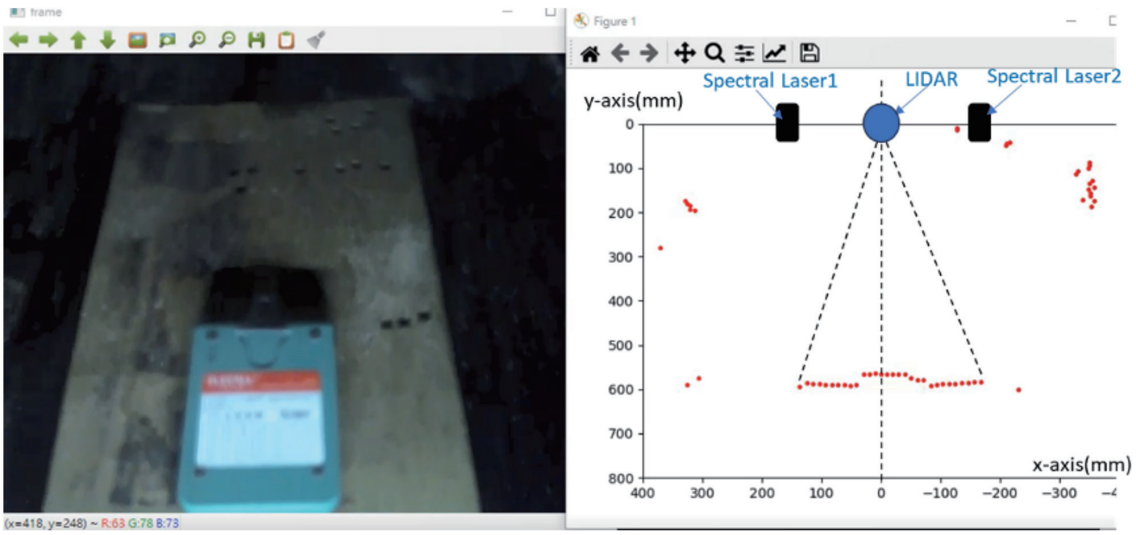

Fig. 10. (Color online) Detection scenario of the target object (toolbox).

experimentation, verifying their outstanding performance during the photovaporization. Moreover, during the pandemic, in-depth research was conducted on laser photovaporization technology for two types of medical waste: masks and rapid screening reagents. The results showed that the CO_2 lasers significantly affected the treatment of rapid screening reagents and masks; this demonstrated the potential of laser technology in medical waste treatment, further enhancing its appeal.

In animal skeletons, the hardness of the skull is second only to that of the teeth. Owing to the small size of the teeth and the absence of skin or muscle covering, it is impossible to directly observe the effects of skin and muscle tissues on bone laser treatment. In this study, we chose to cut animal skulls and meat tissues to ensure the accuracy of the experiment. During the test, the photovaporization method was used to treat the animal's head, producing fine smoke, which was then expelled through an air filtration exhaust system. When using a CO_2 laser for the experiment, it was observed that it exhibited outstanding performance during the photovaporization. The laser almost completely vaporized the skin and meat tissues of the experimental sample, as shown in Figs. 11 and 12.

Regarding medical waste treatment during the pandemic, the primary focus was on masks and rapid screening reagents owing to their large quantities. We focused on these two types of waste, conducting in-depth research using laser photovaporization technology. The laser photovaporization results for rapid screening reagents are shown in Fig. 13. From the experimental results, it can be observed that the CO_2 laser presented excellent results for the treatment of reagents. Specifically, the rapid screening reagents, under the action of the CO_2 laser, achieved significant vaporization results, strongly proving the potential of laser technology in treating reagent waste. Additionally, in this study, we observed that the laser photovaporization for masks also achieved remarkable results. The results for masks are shown in Fig. 14. The laser energy efficiently and almost entirely vaporized the masks, further enhancing the feasibility of using laser technology to treat medical waste.

Fig. 11. (Color online) Illustration of laser vaporization on an experimental sample.

Fig. 12. (Color online) Illustration of laser vaporization on an experimental sample.

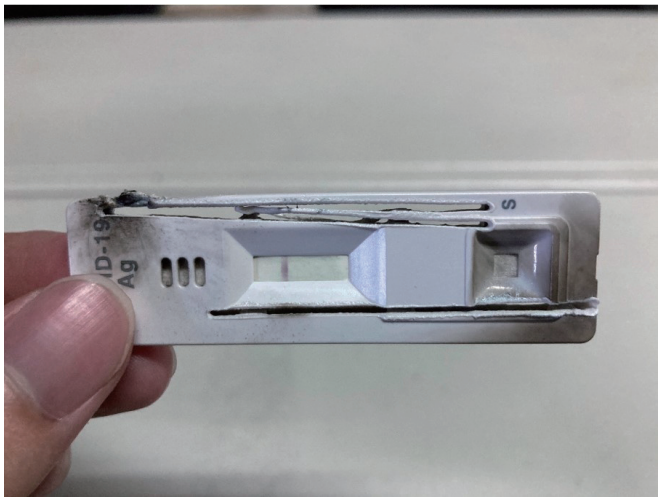

Fig. 13. (Color online) Laser test on medical waste (rapid test reagent).

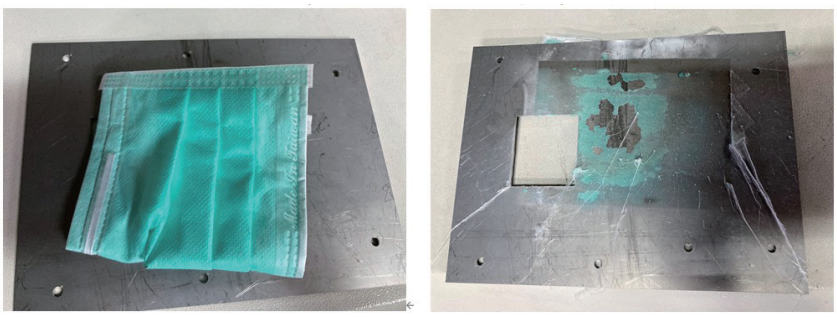

Fig. 14. (Color online) Laser test on medical waste (face masks).

4. Discussion

In this study, we utilized the LiDAR device to locate target objects, allowing this device to determine thresholds on the basis of calculated angles. However, in the current tests, there is a need to optimize the threshold to enhance the accuracy and stability of the entire scanning operation. At the same time, issues arising from insufficient object depth leading to inaccurate detection must be addressed. Although the current 2D LiDAR device is feasible for low-cost object positioning, constructing a complete object shape and feeding it back to the machine are challenging. Therefore, considering more precise positioning scanning, a 3D LiDAR device is an indispensable sensor for the advanced development of the subsequent system.

In terms of the system, we performed preliminary photothermal experiments using lasers to treat meat and bone items, used rapid test reagents, and discarded masks. The test results revealed that CO_2 laser light can feasibly penetrate organic objects instantly. Owing to the extremely high temperature generated by the laser in an instant (about 1000 ℃ or higher), it can instantly penetrate the object in the path of the laser light, splitting it in half. This effect is evident in experiments with rapid test reagents and masks. However, during actual meat gasification tests, the laser could not completely penetrate thicker meat with bones in a single pass. Repeated laser incineration and heating in the area must gradually vaporize it completely.

Furthermore, as discussed in the preliminary tests, the instantaneous energy of laser light can transform matter into heat and gas, allowing it to evaporate and oxidize, resulting in object vaporization. However, for thicker objects, more than instantaneous vaporization is required. Therefore, in the current phase, this research system introduces a beam-splitting system and plans to use two laser beams (one on the left and one on the right) to vaporize the object simultaneously. The aim is to shorten the overall laser movement path by processing from both sides at the same time. Subsequent efforts will focus on using multiple beam-splitting laser heads (approximately ten sets) for vaporization tests, which can significantly increase vaporization efficiency. However, on the basis of the current system design inference, the laser power may decrease or cause losses as the number of beam-splitting sets increases. Hence, as we progress towards multiple beam-splitting heads, we will also require an increase in the wattage of the original laser source to avoid insufficient laser power after splitting.

It remains a research objective for future efforts to enhance laser energy efficiency through preprocessing and to spread the energy density across the entire vaporization range. In current tests, the laser's focus range is limited, making it more suitable for general medical waste treatment. Therefore, photothermal vaporization has preliminary limitations in the current implementation field. However, it is anticipated that advancements in laser technology will significantly resolve the heating issues produced by high-power lasers, making it easier to use multiple laser heads for photothermal vaporization. This would allow objects to be directly subjected to large-area heating, thereby achieving rapid vaporization.

5. Conclusions

We successfully applied CO_2 laser technology in experimental tests on meat products. The laser beam can effectively penetrate objects, providing a possibility for object removal. In terms of the sensing system, low-cost 2D LiDAR technology was chosen and integrated into the multispectral laser ablation machine system. Testing was conducted on a toolbox, and the error was found to be <5 mm (<8%), proving the accuracy of 2D LiDAR positioning in this study. The design of this system not only improved the efficiency of laser ablation but also eliminated the need for manual positioning, further enhancing the level of system automation.

The important results of this study are summarized as follows:

- Through the customized angle range and distance threshold filtering methods, objects within the scanning area were successfully identified.
- Experimental results proved that not only medical masks and rapid test kits can be laser-ablated, but meat products can also undergo laser ablation.
- During the laser ablation of meat products, the carbonization phenomenon on the surface would affect the ablation efficiency. Therefore, increasing the laser power can ensure that the entire object receives effective ablation.
- For different substances, the laser wavelength can be adjusted to increase the absorption efficiency of organic materials by the laser, thereby enhancing the ablation effect.

We demonstrated a promising intelligent object-removal solution. This is the first study to combine laser technology with automation for object ablation applications, and no similar research has been found in the current academic literature. This study not only paved the way for the application of automation technology in environmental protection but also provided valuable references for future related research.

Author Contributions

Conceptualization, C.-Y. P. and M.-H. Y.; methodology, Y.-H. G., C.-Y. P., M.-S. T., and M.-H. Y.; software, Y.-H. G. and M.-S. T.; validation, Y.-H. G., M.-S. T., and , C.-Y. P.; formal analysis, Y.-H. G., M.-S. T., and C.-Y. P.; investigation, J.-P. H. and M.-H. Y.; resources, C.-Y. P. and M.-H. Y.; data curation, Y.-H. G. and M.-S. T.; writing—original draft preparation, J.-P. H. and M.-H. Y.; writing—review and editing, J.-P. H. and M.-H. Y.; visualization, Y.-H. G. and M.-S. T.; supervision, M.-H. Y.; project administration, M.-H. Y.; funding acquisition, C.-Y. P. and M.-H. Y. All authors have read and agreed to the published version of the manuscript.

Funding

The authors acknowledge the support provided for this study by the Ministry of Science and Technology (Grant nos. MOST 111-2221-E167-025-MY2 and MOST 112-2637-H-167-004) of Taiwan.

Conflicts of Interest

The authors declare no conflict of interest.

References

1 R. Lahoz, G. F. De La Fuente, J. M. Pedra, and J. B. Carda: Int. J. Appl. Ceram. Technol. **8** (2011) 1208. https://doi.org/10.1111/J.1744-7402.2010.02566.X
2 L. Cristiano: Infrared Phys. Technol. **102** (2019) 102991. https://doi.org/10.1016/j.infrared.2019.102991
3 E. Khalkhal, M. Rezaei-Tavirani, M. R. Zali, and Z. Akbari: J. Lasers Med. Sci. **10** (2019) 104. https://doi.org/10.15171/JLMS.2019.S18
4 J. H. Kuo, C. L. Lin, J. C. Chen, H. H. Tseng, and M. Y. Wey: Int. J. Greenhouse Gas Control **5** (2011) 889. https://doi.org/10.1016/J.IJGGC.2011.03.001
5 K. L. Hwang, S. M. Choi, M. K. Kim, J. B. Heo, and K. D. Zoh: J. Environ. Manage. **196** (2017) 710. https://doi.org/10.1016/J.JENVMAN.2017.03.071
6 S. Monni: Int. J. Greenhouse Gas Control. **8** (2012) 82. https://doi.org/10.1016/J.IJGGC.2012.02.003
7 S. C. Rowat: Med. Hypotheses. **52** (1999) 389. https://doi.org/10.1054/MEHY.1994.0675
8 P. Lorazo, L. J. Lewis, and M. Meunier: Phys. Rev. B Condens. Matter. **73** (2006) 134108. https://doi.org/10.1103/PHYSREVB.73.134108
9 Y. Zhang and A. Faghri: Int. J. Heat Mass Transf. **42** (1999) 1775. https://doi.org/10.1016/S0017-9310(98)00268-3
10 Y. Xue, L. Cheng, X. Chen, X. Zhai, W. Wang, W. Zhang, Y. Bai, H. Tian, L. Nie, S. Zhang, and T. Wei: PLoS One **13** (2018) 194226. https://doi.org/10.1371/JOURNAL.PONE.0194226
11 T. Wang, Y. Sun, and H. J. Qiu: Infect. Dis. Poverty **7** (2018) 111. https://doi.org/10.1186/s40249-018-0495-3
12 M. Heilmann, A. Lkhagvasuren, T. Adyasuren, B. Khishgee, B. Bold, U. Ankhanbaatar, G. Fusheng, E. Raizman, and K. Dietze: Vet. Sci. **7** (2020) 24. https://doi.org/10.3390/VETSCI7010024
13 Y. Ma, X. Lin, A. Wu, Q. Huang, X. Li, and J. Yan: Waste Dispos. Sustain. Energy **2** (2020) 81. https://doi.org/10.1007/S42768-020-00039-8
14 M. C. M. Alvim-Ferraz and S. A. V. Afonso: Atmos. Environ. **37** (2003) 5415. https://doi.org/10.1016/S1352-2310(03)00572-7
15 COVID-19 has caused a surge in medical waste. Here's what needs to be done: https://www.weforum.org/agenda/2022/02/medical-waste-plastic-environment-covid/ (accessed 21 October 2023).
16 S. M. V. Ngoc, M. A. Nguyen, T. L. Nguyen, H. V. Thi, T. L. Dao, T. M. P. Bui, V. T. Hoang, and D. T. Chu: Case Stud. Chem. Environ. Eng. **6** (2022) 100245. https://doi.org/10.1016/J.CSCEE.2022.100245
17 Health-care waste: https://www.who.int/news-room/fact-sheets/detail/health-care-waste (accessed 21 October 2023).
18 D. Ghorpade, A. D. Thakare, and S. Doiphode: Proc. 2017 Int. Conf. Computing, Communication, Control and Automation. (IEEE, 2017) 1–6.
19 N. M. Fried and D. Fried: Lasers Surg. Med. **28** (2001) 335. https://doi.org/10.1002/LSM.1059
20 M. Forrer, M. Frenz, V. Romano, H. J. Altermatt, H. P. Weber, A. Silenok, M. Istomyn, and V. I. Konov: Appl. Phys. B **56** (1993) 104. https://doi.org/10.1007/BF00325248
21 M. S. Tsai, Y. H. Guan, Y. X. Lin, and M. H. Yen: Proc. 2022 IEEE/ACIS 24th Int. Winter Conf. Software Engineering, Artificial Intelligence, Networking and Parallel/Distributed Computing (IEEE/ACIS, 2022) 140–143.